

Extraction of water bodies from Sentinel-2 imagery in the foothills of Nepal Himalaya

Kumod Lekhak^{1,2} , Pawan Rai³ , Padam Bahadur Budha^{2,*} 

¹ Faculty of Science and Technology, Far Western University, Mahendranagar, NEPAL

² Nepal Environmental Resources Organization, Kathmandu, NEPAL

³ Department of Environmental Science, Goldengate International College, Kathmandu NEPAL

* Corresponding author: B. Budha
E-mail: padambudha88@gmail.com

Received 20.01.2023
Accepted 23.04.2023

How to cite: Lekhal, et al., (2023). Extraction of water bodies from Sentinel-2 imagery in the foothills of Nepal Himalaya, *International Journal of Environment and Geoinformatics (IJEGEO)*, 10(2): 070-081. doi. 10.30897/ijegeo.1240074

Abstract

This paper evaluates an integrated water body mapping method in the Sub-Himalayan region of Nepal using optical imagery of Sentinel-2 satellites of the European Space Agency. This method extracts the information on water bodies by combining image indices, normalized difference vegetation index, and normalized difference water index, using red, green, and near-infrared bands along with slope information to remove false results along the shadow areas. The study results indicated that differentiating indices generated a more accurate map of the water bodies than taking the individual index. The difference in indices enhanced the contrast between water bodies and other environmental features. Based on the accurately mapped water bodies of the study area, this research concluded that the multi-spectral images from the Sentinel-2 can be ideal data sources for water bodies monitoring with finer spatial and temporal resolution. Although smaller water bodies with high vegetation cover cannot be detected by this method, the integrated water body mapping method is suitable for the applications of multi-spectral images in this field.

Keywords: feature extraction, image threshold, Kanchanpur, STEP accuracy, water indices

Introduction

Water, an important and essential part of the ecosystem, is responsible for the development and growth of life forms on Earth (Biggs et al., 2017) and covers more than three-quarters of Earth's surface. The amount and location of inland surface water play a vital role in decision-making for policymakers (Biggs et al., 2017; Du et al., 2016; Verpoorter et al., 2014). These surface waters are very susceptible to change (Nazari-Sharabian et al., 2018) and are, therefore, responsible for various environmental and ecological modifications (Habitat, 2013, 2015; Villamagna and Murphy, 2010), as well as human socio-economic development (Biggs et al., 2017; Habitat, 2015; Nazari-Sharabian et al., 2018; Villamagna and Murphy, 2010). As a crucial part of the global climate cycle, mapping water bodies, especially fresh water, is an essential task and a requisite (Biggs et al., 2017; Du et al., 2016). This mapping of freshwater in the spatiotemporal domain, describing the distribution of water bodies in space and time, makes the task essential for academic research and policy-making (Du et al., 2016; Verpoorter et al., 2014; Weise et al., 2020).

With the development and increasing applications of satellite imagery in recent years, the mapping of natural resources, like forest and water bodies, is gaining much importance (Verpoorter et al., 2012, 2014; F. Yang et al., 2017). In addition, geospatial tools are advantageous for identifying natural resources, such as forest and water bodies, and assessing their status (S. W. Wang et al., 2020; Yan et al., 2020; F. Yang et al., 2017). Moderate-

resolution Imaging Spectro-radiometer (MODIS) images have been widely used to map water bodies at both global and regional scales (Colditz et al., 2018; Liu et al., 2020; Y. Wang et al., 2020; Xing and Niu, 2019). For regional studies, images provided by the Landsat TM (Thematic Mapper) and ETM+ (Enhanced Thematic Mapper Plus) proved to be valuable as the imagery has a moderate spatial resolution (30 m), provides multispectral images (seven or eight bands), with a short revisit interval (16 days) and includes decades of records (Du et al., 2016; Masocha et al., 2018; Zhai et al., 2015). Various techniques have been adopted and developed to delineate water bodies in remotely sensed imagery and are commonly grouped into three categories, i.e., Spectral bands (Verpoorter et al., 2012, 2014; Zhai et al., 2015; Kavzoğlu et al., 2023), classification (Acharya et al., 2018; Huang et al., 2018; Talukdar et al., 2020; Kavzoğlu, et al., 2021) and index-based extraction (Acharya et al., 2018; Du et al., 2016; F. Yang et al., 2017; Gazioğlu, 2018).

Analyzing spectral bands helps to identify water bodies by applying thresholds to one or more spectral bands. Thresholding individual band is easy to implement but often misclassifies mountain shadows, urban areas, or other background noise as water bodies (Verpoorter et al., 2012). Spectral analysis can distinguish natural entities from artificial entities but cannot differentiate the variation within the former. While the classification process helps to extract water bodies from images by applying machine learning algorithms. Algorithms such as maximum-likelihood classifiers, decision trees,

artificial neural networks, support vector machines, K-means, and iterative self-organizing data analysis (ISODATA) (González-González et al., 2022; Lu and Weng, 2007; Otukei and Blaschke, 2010) have been used for this method. Classification approaches may achieve higher accuracy than spectral band methods under some circumstances; however, expert experience or existing reference data are required to select appropriate training samples, which prevents these methods from being applied over large areas (González-González et al., 2022). Index-based water boundary extraction uses various spectral bands through various algebraic operations to enhance the distinctions between water bodies and land. The most commonly used indices are the Normalized Difference Vegetation Index (NDVI) and Normalized Difference Water Index (NDWI). However, due to the similar spectral response trend between the mountain shadow area and vegetation-

covered area, as well as water bodies and artificial sites in these two indices, NDVI or NDWI alone cannot be used to eliminate the interference of the shadow of the mountain, and the artificial construction land, during the process of the water body mapping (Lu and Weng, 2007; F. Yang et al., 2017). These factors make it a challenging assignment to map water bodies in the Himalayan region (Acharya et al., 2018). Therefore, there is a paucity of studies in the inventory and mapping of water bodies (Acharya et al., 2018; Bhujju et al., 2010; Liu et al., 2020). The purpose of this paper is to evaluate the potential of the integrated method using Sentinel -2A satellite imagery data to be used in delineating boundaries of water bodies and to find an optimal mapping method so that this type of data can be used for high temporal and spatial resolution water bodies monitoring in the future.

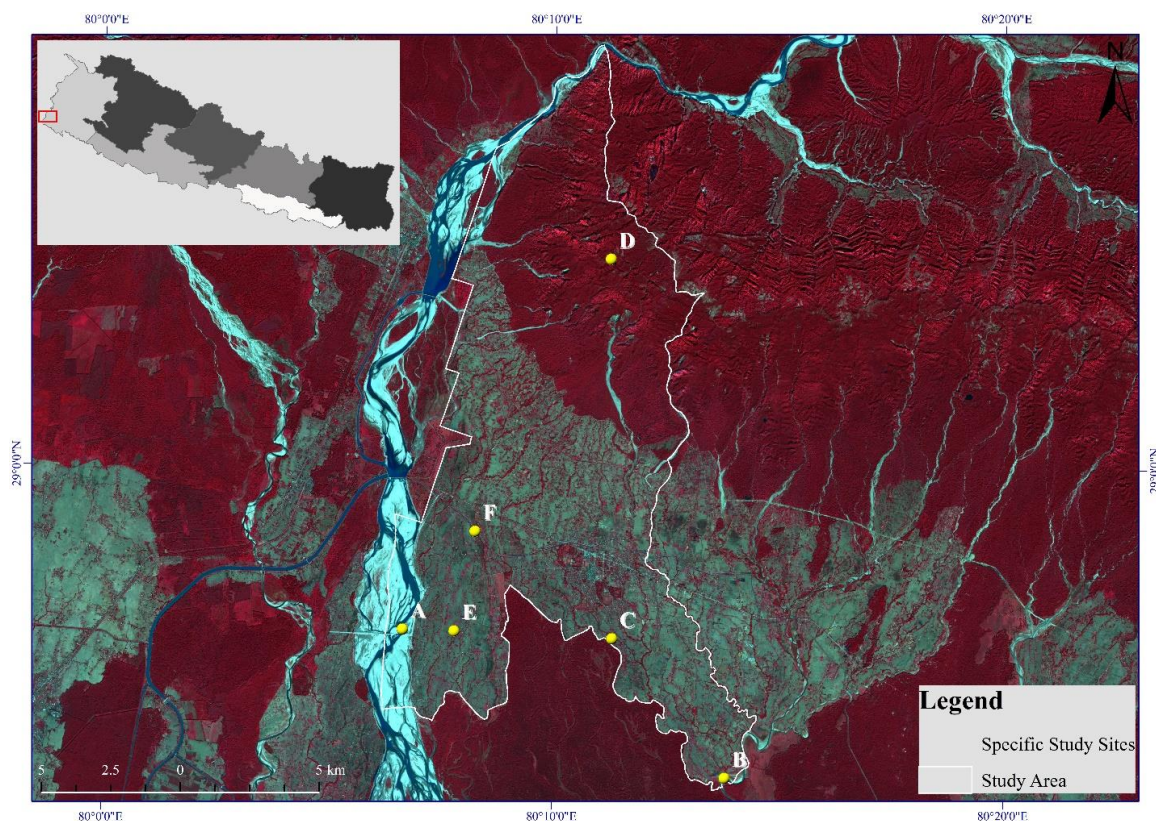


Fig. 1: Study Area Location and Specific Field Sites (Inset: Nepal with provinces; experimental area in red box)

Materials and Methods

Study Area

The Bhimdatta municipality, covering an area of 171.14 km², was selected as the research site for this study. The study area is located in the Southwestern corner of Nepal in Sudurpaschim Province, sharing a border with India in the south and west (Figure 1). This region is characterized by a large river with its floodplains (Mahakali River), dense tropical forest, expansive grassland, small rivers/rivulets, and canals, making the area better supplied by irrigation and drainage system for agricultural production. The human population density is very high compared to the neighboring cities. Large

parts of the forest and natural grassland have been converted into settlement and agricultural land.

The study was conducted in selected locations of varying landforms from the Tarai and Siwalik regions of the Bhimdatta Municipality. Also, these sites depicted varying land use attributes whose details can be observed in Table 1.

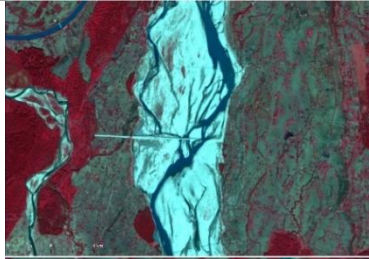

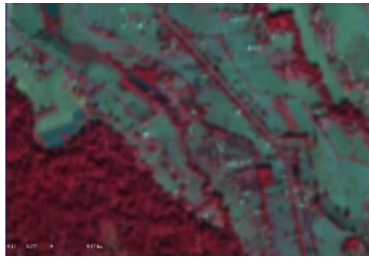



Data and Image Pre-Processing

For this study, multispectral images of the Sentinel-2 satellite were acquired from the online data portal of the European Space Agency (ESA). The image data downloaded were dated from November and December, the post-monsoon period in Nepal, since permanent

water bodies are easily distinctive in post-monsoon season (Huang et al., 2018) Besides, all the sub-scenes of the data were all free of clouds which would otherwise obscure the underlying ground features. Imagery from dry periods generates more cloud-free data and results in higher accuracy in the data analysis (Huang et al., 2018; Yan et al., 2020). Along with satellite imagery, this study uses digital elevation model (DEM) data obtained

from ALOS PALSAR radiometrically terrain-corrected products having a resolution of 12.5m. Besides, high spatial resolution Google Earth images were used as references for the accuracy assessment. The acquisition dates of the Google Earth reference data and Sentinel-2 images were matched to minimize errors in the surface water bodies that may happen due to temporal variations.

Table 1: Description of Specific Study Area

Sites	Image
A Chadani-Dodhara (Mahakali River: Snow fed Perennial River)	
B Baghpanta (Chaudhar River: Siwalik Originated River)	
C Gobariya (Near Suklaphanta National Park: Groundwater fed River)	
D Jhilimila Lake (Natural Ponds/Lake in Siwalik hills)	
E Ayri (An Artificial Pond)	
F Bangaun (Mahakali Irrigation Canal)	

Data and Image Pre-Processing

A bundle of Sentinel-2 imagery consists of 13 multispectral bands with varying resolutions of 10 m, 20 m, and 60 m. Images were atmospherically corrected using the Sen2Cor algorithm, available in the Sentinel

Application Platform (SNAP) toolbox provided by ESA. Bands having a spatial resolution of 10 m, Green band (B3), Red band (B4), and Near-infrared band (B8) were considered for the calculation of indices applied in water body extraction.

Table 2: Band Information of Sentinel-2 Satellite Images

Band	Resolution	Central Wavelength	Description
B1	60 m	443 nm	Ultra Blue (Coastal and Aerosol)
B2	10 m	490 nm	Blue
B3	10 m	560 nm	Green
B4	10 m	665 nm	Red
B5	20 m	705 nm	Visible and Near Infrared (VNIR)
B6	20 m	740 nm	Visible and Near Infrared (VNIR)
B7	20 m	783 nm	Visible and Near Infrared (VNIR)
B8	10 m	842 nm	Visible and Near Infrared (VNIR)
B8a	20 m	865 nm	Visible and Near Infrared (VNIR)
B9	60 m	940 nm	Short Wave Infrared (SWIR)
B10	60 m	1375 nm	Short Wave Infrared (SWIR)
B11	20 m	1610 nm	Short Wave Infrared (SWIR)
B12	20 m	2190 nm	Short Wave Infrared (SWIR)

Methods**Generation of Indices**

The first task in the extraction of water bodies was to determine the NDVI (vegetative index) and NDWI (water index) using Near-infrared (NIR), Red, and Green bands of Sentinel-2 data. Along with these indices, a slope map was also prepared. These indices permitted the separation of water bodies from other land use features (Acharya et al., 2018; F. Yang et al., 2017). However, NDWI was inefficient in extracting shallow water bodies and couldn't separate built-up structures from water features (F. Yang et al., 2017). Therefore, this research has used both NDWI and NDVI, which were summed to increase the detail of water features. The slope was used to eliminate the impacts of mountain shadows that were mapped as water bodies. As the surface of water bodies is more gentle than the shadows cast by mountains in steep areas (Jawak and Luis, 2015; F. Yang et al., 2017), false water bodies from such shadows can be removed by the application of slope threshold.

As the water bodies in the NDVI index are generally negative or closer to zero, this index can be applied to map water bodies by thresholding (Brakenridge and Anderson, 2006; Zhan et al., 2002). NDWI effectively reduces the effects of vegetation and highlights more information on water bodies (McFeeters, 1996; Suwarsono et al., 2021). The equations to estimate these

indices are presented in Table 3. The reflected radiance of an object captured by a sensor in remote sensing depends upon the extent of electromagnetic radiation absorbed by that object; i.e., the more it absorbs, the less it reflects (Merry, 2001; Rabinskiy et al., 2020)..

The water body absorbs more in the infrared region (Jawak and Luis, 2015), making its reflected radiance very low in infrared and short-wave-infrared bands, distinguishing water from other features like vegetation, buildings, bare soil, and roads that have higher reflectance in the same wavelength region. The reflectance of water in the NIR band is less than in the Green and Red bands. These two properties emanated by analyzing the pixel values are valid for water bodies but not for other objects like soil, sand, roads, vegetation, or buildings. Hence by applying these two peculiarities, water bodies can be easily extracted. The selection of these wavelengths maximizes the reflectance properties of water (McFeeters, 1996). Hence, the estimation of NDWI maximizes the typical reflectance of water features by using green wavelength, whereas it minimizes the low reflectance of NIR by water features (Yan et al., 2020).

These indices generated water-covered areas but with some false positives in steep surfaces; however, slope, a DEM-derivative, was applied with a suitable threshold to remove water bodies of such sites with high gradients.

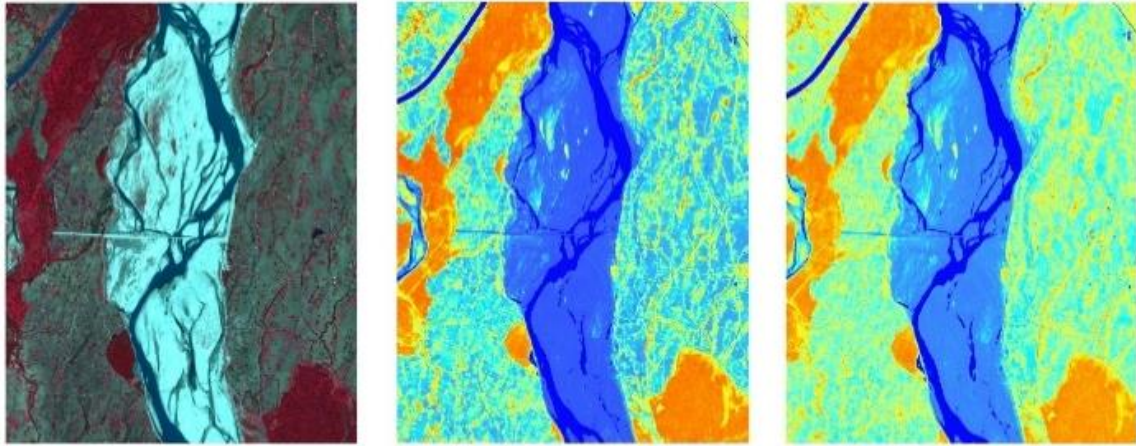


Fig. 2: Generation of NDVI and NDWI indices from Sentinel-2 image for site A

Table 3: Summary of the Indices Used For Extraction of the Water Body

Index	Description	Remarks
Normalized Difference Vegetation Index (NDVI)	$NDVI = \frac{NIR - Red}{NIR + Red}$	NIR and Red are near-infrared band and red band reflectance, respectively. They correspond to band 8 and band 4 on Sentinel-2 images
Normalized Difference Water Index (NDWI)	$NDWI = \frac{Green - NIR}{Green + NIR}$	Green and NIR are green band and near-infrared band, respectively. They correspond to band 3 and band 8 on Sentinel-2 images.

Thresholding

Thresholding is an essential step in water body mapping that differentiates them from the background features. Due to the dynamic nature of image variables such as spectral indices and devoid of any general methodology for getting image segmentation, difficulties have arisen in obtaining optimum threshold values (Bangira, 2019; Bangira et al., 2019). Furthermore, threshold values can vary temporally and spatially among regions, depending on different images and characteristics of water bodies (F. Yang et al., 2017). Several methods are available for the segmentation process of image indices which can be broadly associated with either region-based or edge-based segmentation methods for thresholding. Histogram shape-based methods (Basar et al., 2020; Pare et al., 2020), clustering-based methods (Al-Rahlawee and Rahebi, 2021; Otsu, 1979; P. Yang et al., 2020), entropy-based methods (Pandey et al., 2018; Pare et al., 2020) are some of the commonly used segmentation methods.

These methods either underestimate or overestimate the surface water sources. Although threshold segmentation can differentiate water pixels, the processes have been known to yield inconsistent results in situations where the spectral characteristics between water and other dark objects, such as buildings and shadows, are similar (Sezgin and Sankur, 2004).

As threshold values, applied to distinguish water from non-water, were unstable and varied with scene and location and miscellaneous uncertainty in available methods, the histogram shape-based method was used to select thresholds for this research. After drawing the spectral curves of typical features based on the imageries of NDVI, NDWI, and NIR bands, the data range of feature samples based on different indices to select the endpoint values (or values closing to the endpoints) or the logical values i.e., water > 0; third, comparing the result imageries of each alternative visually to find the better one.

The images formed after the computation of the indices were converted into a binary map with respect to the threshold value of water bodies. This binary map converts an image with value one, representing a water body, and zero, indicating non-water features. This map preparation supported selecting the threshold for the output function. Also, this canceled the diminishing effect of the negative values while calculating the weighted sum. The thresholding is a critical factor affecting ground-feature extraction using the index-based method. Previous scholars applied the default threshold to classify the indices image (Du et al., 2016; Yan et al., 2020; F. Yang et al., 2017; Zhai et al., 2015). However, the default threshold value can inhibit the index-based methods from achieving the best mapping result.

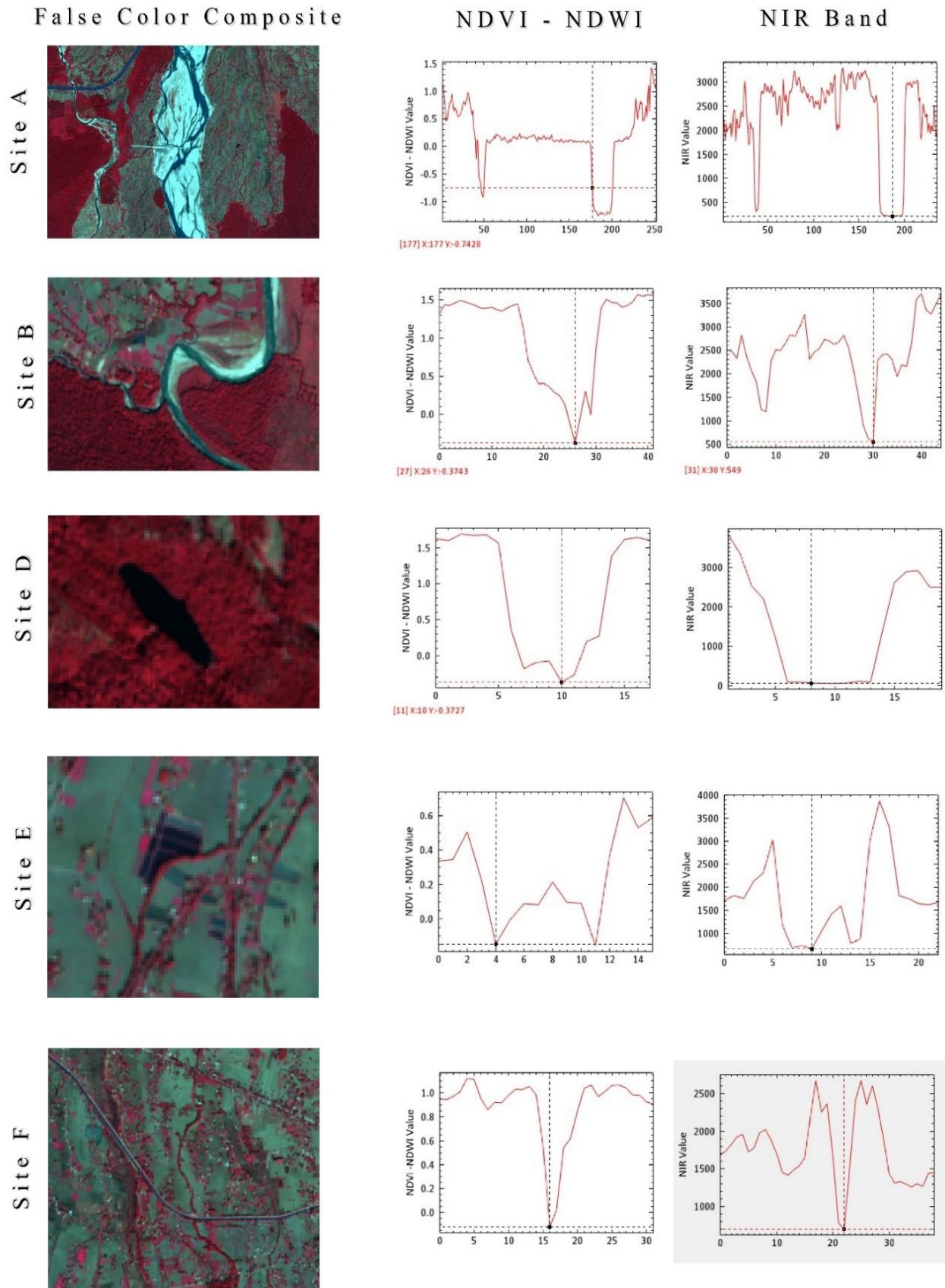


Fig. 3: Threshold Value selection for NDVI-NDWI and NIR Images for various types of Water Bodies in the study area

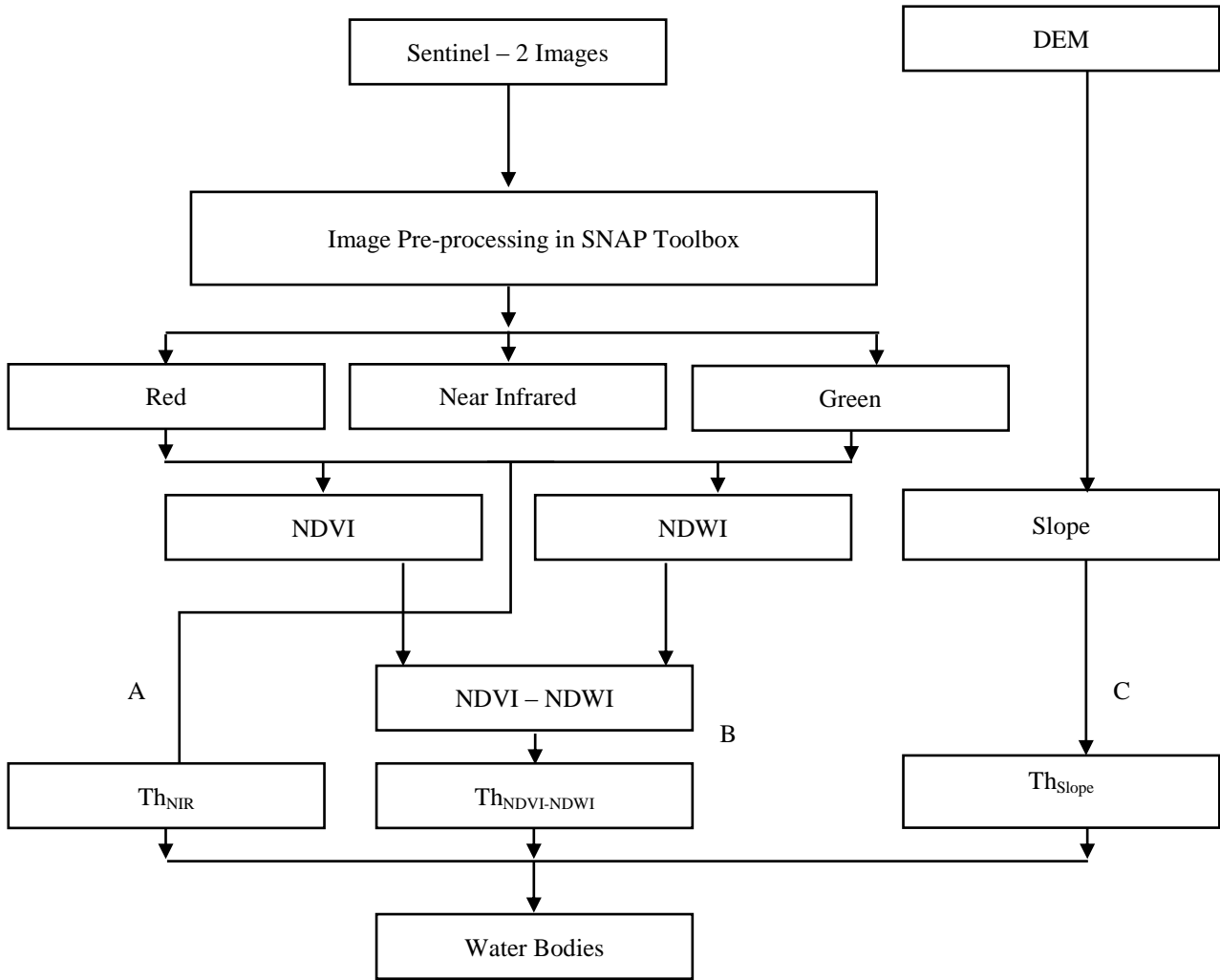


Fig. 4: Methodological approach to extract water bodies by using index-based water body mapping method based on Sentinel 2 imagery. A, B, and C are threshold values of the NIR band, NDVI – NDWI, and Slope, respectively. ThNIR, ThNDVI-NDWI, and ThSlope are thematic maps that are generated from the NIR band, NDVI–NDWI index, and Slope used to extract water body.

Validation and Accuracy Assessment

The overall performance of the index-based method to extract water bodies was verified by visual inspection and pixel-by-pixel assessment of extracted images with reference images. Subsequently, a detailed appraisal of the results was conducted by using Shape-Theme-Edge-Position (STEP) matrices (Lizarazo, 2014) to assess the performance of the method in identifying the water body. Thus, here evaluation of extracted water bodies was conducted through a hybrid approach of the classical confusion matrix and the recent STEP matrix.

A confusion matrix was utilized to evaluate Producer Accuracy (PA), User Accuracy (UA), Overall Accuracy (OA), and Kappa Accuracy using the following equations:

$$PA = \frac{TP}{TP+FN}$$

Where,

TP = Total number of Correct Extraction

FN = Total Number of Water Pixel not Detected

$$UA = \frac{TP}{TP+FP}$$

Where,

FP = Total Number of Incorrect Extraction

$$OA = \frac{TP+TN}{T}$$

TN = Total Number of Non Water Bodies that are Correctly Rejected

T = total number of pixel in experimental scene of Sentinel-2 image

$$Kappa = \frac{T \times (TP \times TN) - \Sigma}{T \times T \Sigma}$$

Where,

$$\Sigma = (TP + FP) \times (TP + FN) \times (FN + TN) \times (FP + TN)$$

Here TP, FN, TN, and FP are categorized pixels by comparing the extracted water pixel with a reference image.

Extraction of the water body with its distinct boundary is the central part of this research which should be correctly done. Classic accuracy by confusion matrix could not reflect the accuracy of boundary conditions for the water bodies. Thus, the evaluation of boundary conditions was conducted using the area-based accuracy

(STEP) method (Lizarazo, 2014). The final results were compared with reference images, and their shape similarity, theme similarity, edge similarity, and position similarity were estimated. The equations for evaluating these four parameters of STEP accuracy are presented in Table 4.

Table 4: STEP method for accuracy assessment (Lizarazo, 2014)

Accuracy Measure	Equation	Remarks
Shape Similarity	$S = r_{npi}k$	Where, r_{npi} is the ratio of the classified object's normalized perimeter index (NPI) to the reference object's NPI, and k is given the value +1 when r_{npi} is less than or equal to 1. 0, and the value -1 otherwise. S values range from 0 to 1.
	$NPI = P_{eac}/P_{obj}$	Where, P_{eac} perimeter of the equivalent area circles (eac), P_{obj} is the object's perimeter. A regular shape (i.e. a circular object) will have an NPI of 1 and less compact regions' values will be lesser than 1.
Theme Similarity	$T = A_{int}/A_{ref}$	Where, A_{int} is the area of the geometric object representing the point set intersection between the classified object and the reference object, and A_{ref} is the area of the reference object's geometry. T values range in the between 0 and 1 interval. A classified object that completely covers the reference object and matches its thematic category has a value of 1.
Edge Similarity	$E = (l_{int}/p_{ref})^k$	Where, l_{int} is length of the boundary of the geometric object representing the point set intersection between the boundary of the classified object and the boundary of the reference object, p_{ref} is the perimeter of the reference object, and k is given the value +1 when l_{int} is less than or equal to p_{ref} , and the value -1 otherwise.
Position Similarity	$P = 1 - d_{cent}/d_{cac}$	Where, d_{cent} is euclidian distance between the centroid of a reference object and the centroid of the corresponding classified object(s), and d_{cac} is the diameter of the combined area circle. P values range in the interval of 0 and 1. A classified object with a correctly predicted position has a value of 1.

Results and Discussion

Water Body Mapping Performance (Visual Interpretation)

The performance of the water body extraction method was evaluated by observing their variation with the reference data. The final extracted map was overlaid with reference images to identify the accuracy of the technique implemented. In Figure 5, it can be observed the display of results overlaid with reference images. The visual interpretation indicated that the applied method successfully extracted most of the water bodies in the area. Successful extraction of water bodies was observed in large and open water bodies such as the Mahakali River, the Mahakali Irrigation Canal that goes to India, the Chaudhar River, and Jhilimila Lake. A little difference was observed between the reference images and the final extracted data, and the boundaries in such water bodies were conspicuous. In a few cases, underestimation and overestimation of water bodies were observed in the study area. This method underestimates the boundary delineation of the smaller streams, rivers with high vegetative cover, and small ponds while

overestimating the water bodies in an urban center such as Mahendranagar. This justified the error associated with NDWI in water body extraction mapping. This signified NDWI only would result in inaccurate water body extraction in urban centers and casted mountains shadows (Acharya et al., 2018; F. Yang et al., 2017).

Accuracy of Mapping

The accuracy of water body extraction was observed for various types of water bodies in the study area. Table 5 shows the extraction accuracy and Kappa statistics of the water bodies mapped. The accuracy was higher and congruent for most water body categories except for the groundwater-fed streams. OA ranges from 80.4% to 97.9%, whereas the Kappa coefficient was between 0.63 and 0.95. With a kappa value of 0.95, large water bodies like the snow-fed river (Mahakali River in Site A) yielded more accurate results than the smaller and shallower water bodies such as the irrigation canal (Site F). On the other hand, the index-based method was found inadequate in extracting the groundwater-originated river of the Terai region.

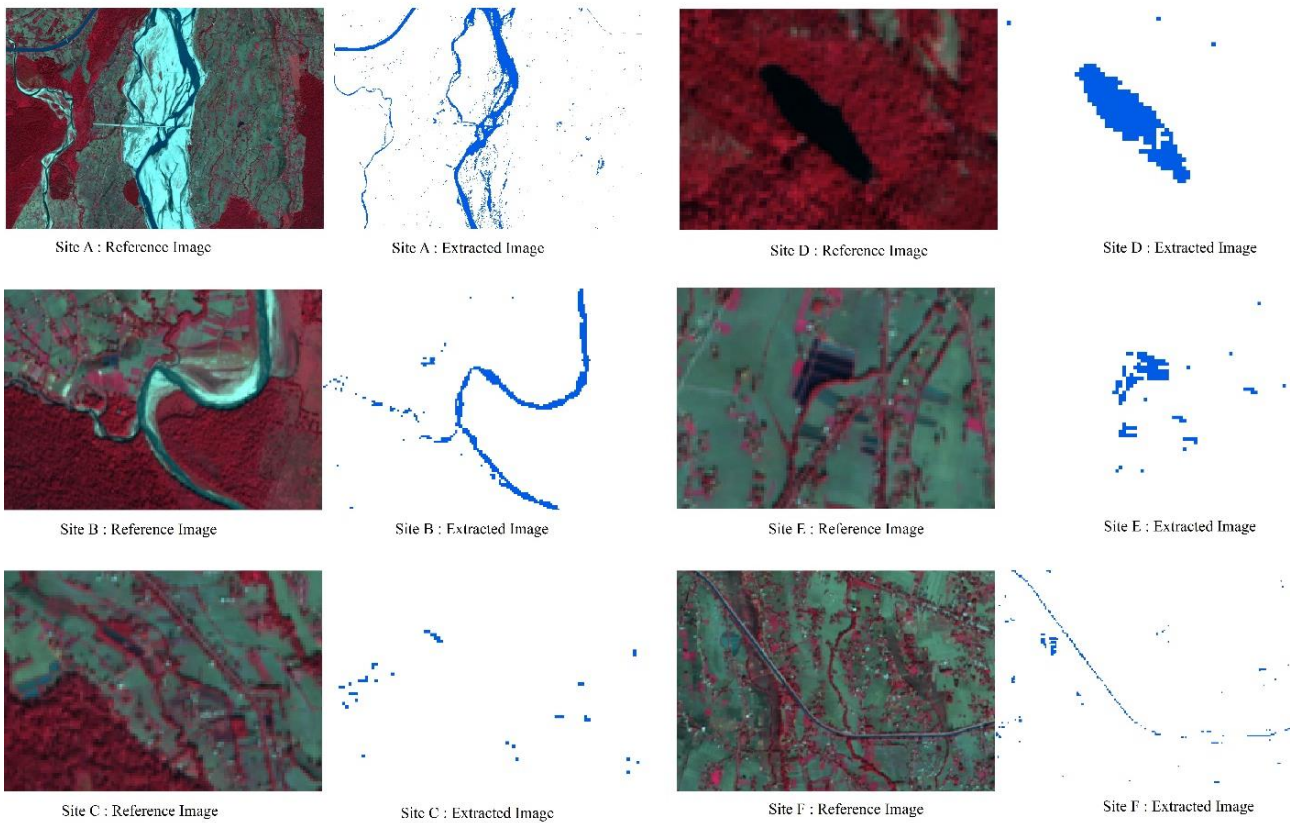


Fig. 5: Comparison of Reference Image with Final Water Body Extraction Mapping Results for an Experimental sites

Table 5: Water mapping accuracy assessment results for various experimental sites using Sentinel-2 image

Experimental Site	PA	UA	OA	Kappa
Site A (Snow fed River)	97.1%	96.9%	97.9%	0.95
Site B (Mountain fed River)	95.2%	86.6%	85.3%	0.86
Site C (Groundwater fed River)	-	-	-	-
Site D (Natural Lake)	97.8%	95.8%	96.4%	0.85
Site E (Artificial Ponds)	82.7%	82.7%	92.7%	0.82
Site F (Irrigation Canal)	81.8%	86.3%	80.4%	0.63

This study showed that large water bodies (Snow fed Mahakali River, Natural Lakes) achieve higher PA of 97.1%, OA 97.9%, and Kappa coefficient of 0.95 on the extracted information. The reason for this result is that the background of the large water bodies had been contrasting with its surroundings, along with its high resolution, the information of large water bodies can be extracted more accurately by the given integrated index method (Du et al., 2016; Kaplan and Avdan, 2017). Moderate-sized water bodies such as the Chaudhar (a mountain-fed river) depicted good extraction accuracy with PA of 95.2%, OA of 85.3%, and Kappa coefficient

of 0.86; but, such water bodies failed to explain the thematic and positional similarity. On the other hand, water bodies such as groundwater-originated streams and irrigation canals indicated PA of 81.8%, OA of 80.4%, and Kappa coefficient of 0.63. The relatively narrow water bodies with a width of less than 10m pixels couldn't be enhanced by the NDVI-NDWI index; therefore, such water areas were not precisely delineated by this method (Suwarsono et al., 2021).

Commonly used classification accuracy does not justify the water bodies in thematic and geometric dimensions (Budha and Bhardwaj, 2019). Thus, object-based classification accuracy (STEP method) was used to define the thematic and geometric accuracies. STEP method was used to understand the reliability of thematic attributes (shape, theme, edge, and positional similarity) carried by classified objects (Budha and Bhardwaj, 2019; Lizarazo, 2014). The STEP accuracy analysis presented that thematically larger water bodies (snow fed Mahakali River, natural lakes) can be extracted more accurately than smaller water bodies (irrigation canals, artificial ponds). The background of the the large water had been contrasting with its surroundings, along with its higher resolution, the information about large water bodies can be extracted more accurately by the given integrated index method (Du et al., 2016; F. Yang et al., 2017). Table 6 shows the accuracy measures obtained from STEP accuracy analysis.

Shape similarity was observed with lower values in larger water bodies such as braided snow-fed rivers followed by artificial ponds. It was found higher in

compacted large natural lakes and mountain-originated rivers. The geometric form of spatial objects helped to describe the shape of the extracted region based on how it deviated from the specified geometry, i.e., circle (used in this study), square, or triangle (Cai et al., 2018; Lizarazo, 2014). In braided water bodies of large rivers, sand pixels are mixed with water pixels leading to an overestimation of water bodies within the flood plain. On the other hand, the mixed vegetation cover along artificial ponds obscured the water pixels leading to an underestimation of water bodies. Thematic properties of spatial objects refer to non-metric attributes such as natural lakes, artificial ponds, and river water categories. It describes how well the classified objects represent categories assigned to reference objects. Natural large water bodies (snow-fed rivers and natural lakes) had a high value of thematic similarity index as they overlapped almost entirely with the reference objects. The extracted information of smaller water bodies had a lower thematic similarity value as it did not completely coincide with the reference objects. The edge or boundary can be defined as the set of line segments that represent the limit of an entity (Aher et al., 2017; Kaplan and Avdan, 2017). The extracted information on mountain-originated rivers had excellently performed when considering the exterior and interior boundaries of corresponding objects despite just optimum accuracy in detecting boundaries of water bodies of other types. The direct position of an object can be described by a single set of coordinates (Lizarazo, 2014) within a coordinate reference system. A position similarity index considers the centroid position of classified and reference objects. Due to the smaller size of the irrigation canal and the meandering nature of the mountain-fed river, this index is lower. The positional accuracy for all other types of water bodies is excellent.

Table 6: STEP Metrics For Classified Water Bodies Using Integrated Index Method.

Experimental Site	Shape Similarity	Theme Similarity	Edge Similarity	Position Similarity
Site A (Snow fed River)	0.20	0.83	0.69	0.99
Site B (Mountain fed River)	0.71	0.52	0.99	0.20
Site C (Groundwater fed River)	-	-	-	-
Site D (Natural Lake)	0.77	0.86	0.83	0.97
Site E (Artificial Ponds)	0.30	0.57	0.60	0.78
Site F (Irrigation Canal)	0.52	0.17	0.75	0.57

For an appraisal of the performance of Sentinel-2 images using the index method presented here, the procedure was applied in a similar region. The test was conducted

in locations like Chitwan Valley and Morang District, which have identical physiography to the study site. The test study showed promising results that were similar to the calibration sites. The accuracy of the results obtained from the Chitwan region was 91.39%, and that of the Morang region was 97.42%, respectively estimated using a classical confusion matrix. Positional accuracy was lower in Chitwan which can be attributed to the overestimation of water bodies that stand specifically near high built-up density areas. Whereas the accuracy in the Terai region was observed highly comparable to that of the experimental site.

Conclusion

The multispectral Sentinel-2 images have higher spatial as well as temporal resolution when compared to similar freely available satellite datasets. Such features make Sentinel-2 imagery highly effective in information extraction regarding the dimensions of water bodies and monitoring their changes. In this method, integrated index-based waterbody extraction, various thresholds were applied in different sites in each calibrated and test site. As the indices are sensitive to varying environmental components, thresholding should be done before the enactment of the method. Although the results were satisfactory in different experimental and test sites, some issues remain to be considered. There are issues such as shadow due to the sun's height and mountain topography, atmospheric conditions, water bodies' state of pollution, and eutrophication. All of these factors affect the reflection activity of water bodies, which subsequently impacts the extraction of water bodies. This has been observed in test Chitwan and Morang, which affects the overall accuracy of water body extraction. This study assesses the applicability of the semi-automated water-based index techniques in delineating the extent of water bodies in the various area of foothills of the central Himalayas using Sentinel-2 multispectral data. The study revealed that the identification of the optimum threshold value should be used to extract water bodies efficiently from Sentinel-2 data.

References

- Acharya, T. D., Subedi, A., Lee, D. H. (2018). Evaluation of water indices for surface water extraction in a landsat 8 scene of Nepal. *Sensors (Switzerland)*, 18(8), 1–15. <https://doi.org/10.3390/s18082580>
- Aher, S., Kantamaneni, K., Deshmukh, P. (2017). Detection and Delineation of Water Bodies in Hilly Region using CartoDEM SRTM and ASTER GDEM Data. *Remote Sensing of Land*, 1(1), 41–52. <https://doi.org/10.21523/gcj1.17010103>
- Al-Rahlawee, A. T. H., Rahebi, J. (2021). Multilevel thresholding of images with improved Otsu thresholding by black widow optimization algorithm. *Multimedia Tools and Applications*, 80(18), 28217–28243.
- Bangira, T. (2019). Mapping surface water in complex and heterogeneous environments using remote

- sensing. Stellenbosch: Stellenbosch University.
- Bangira, T., Alfieri, S. M., Menenti, M., Van Niekerk, A. (2019). Comparing thresholding with machine learning classifiers for mapping complex water. *Remote Sensing*, 11(11), 1351.
- Basar, S., Ali, M., Ochoa-Ruiz, G., Zareei, M., Waheed, A., Adnan, A. (2020). Unsupervised color image segmentation: A case of RGB histogram based K-means clustering initialization. *Plos One*, 15(10), e0240015.
- Bhujju, U. R., Khadka, M., Neupane, P. K., Adhikari, R. (2010). A Map Based Inventory of Lakes in Nepal. *Nepal Journal of Science and Technology*, 11, 173–180. <https://doi.org/10.3126/njst.v11i0.4141>
- Biggs, J., Von Fumetti, S., Kelly-Quinn, M. (2017). The importance of small waterbodies for biodiversity and ecosystem services: implications for policy makers. *Hydrobiologia*, 793(1), 3–39.
- Brakenridge, R., Anderson, E. (2006). MODIS-based flood detection, mapping and measurement: the potential for operational hydrological applications. In *Transboundary floods: reducing risks through flood management* (pp. 1–12). Springer.
- Budha, P. B., Bhardwaj, A. (2019). Landslide Extraction from Sentinel-2 Image in Siwalik of Surkhet District, Nepal. *ISPRS Annals of the Photogrammetry, Remote Sensing and Spatial Information Sciences*, 4(5/W2), 9–15. <https://doi.org/10.5194/isprs-annals-IV-5-W2-9-2019>
- Cai, L., Shi, W., Miao, Z., Hao, M. (2018). Accuracy assessment measures for object extraction from remote sensing images. *Remote Sensing*, 10(2). <https://doi.org/10.3390/rs10020303>
- Colditz, R. R., Souza, C. T., Vazquez, B., Wickel, A. J., Ressler, R. (2018). Analysis of optimal thresholds for identification of open water using MODIS-derived spectral indices for two coastal wetland systems in Mexico. *International Journal of Applied Earth Observation and Geoinformation*, 70, 13–24.
- Du, Y., Zhang, Y., Ling, F., Wang, Q., Li, W., Li, X. (2016). Water bodies' mapping from Sentinel-2 imagery with Modified Normalized Difference Water Index at 10-m spatial resolution produced by sharpening the swir band. *Remote Sensing*, 8(4). <https://doi.org/10.3390/rs8040354>
- Gazioğlu, C. (2018). Biodiversity, Coastal Protection, Promotion and Applicability Investigation of the Ocean Health Index for Turkish Seas. *International Journal of Environment and Geoinformatics*, 5(3), 353-367, doi. 10.30897/ijegeo.484067
- González-González, A., Clerici, N., Quesada, B. (2022). A 30 m-resolution land use-land cover product for the Colombian Andes and Amazon using cloud-computing. *International Journal of Applied Earth Observation and Geoinformation*, 107, 102688.
- Habitat, U. N. (2013). State of the world's cities 2012/2013: Prosperity of cities. Routledge.
- Habitat, U. N. (2015). Habitat III issue paper 22—informal settlements. New York: UN Habitat.
- Huang, C., Chen, Y., Zhang, S., Wu, J. (2018). Detecting, extracting, and monitoring surface water from space using optical sensors: A review. *Reviews of Geophysics*, 56(2), 333–360.
- Jawak, S. D., Luis, A. J. (2015). A Rapid Extraction of Water Body Features from Antarctic Coastal Oasis Using Very High-Resolution Satellite Remote Sensing Data. *Aquatic Procedia*, 4(Icwrcoe), 125–132. <https://doi.org/10.1016/j.aqpro.2015.02.018>
- Kaplan, G., Avdan, U. (2017). Mapping and Monitoring Wetlands Using Sentinel-2 Satellite Imagery. *ISPRS Annals of the Photogrammetry, Remote Sensing and Spatial Information Sciences*, 4(4W4), 271–277. <https://doi.org/10.5194/isprs-annals-IV-4-W4-271-2017>
- Kavzoğlu, T., Yılmaz, E., Ö., Çölkesen, İ., Sefercik, U. G., Gazioğlu, C. (2023). Detection and Monitoring of Mucilage Formations Using Pixel Based Convolutional Neural Networks: The Case Study of Izmit Gulf, Turkey, *Mucilage Problem in the Sea of Marmara*, 233-251.
- Kavzoğlu, T., Tonbul, H., Çölkesen, İ., Sefercik, U. G. (2021). The Use of Object-Based Image Analysis for Monitoring 2021 Marine Mucilage Bloom in the Sea of Marmara. *International Journal of Environment and Geoinformatics*, 8(4), 529-536, doi.10.30897/ijegeo.990875
- Liu, C., Shi, J., Liu, X., Shi, Z., Zhu, J. (2020). Subpixel mapping of surface water in the Tibetan Plateau with MODIS data. *Remote Sensing*, 12(7), 1154.
- Lizarazo, I. (2014). Accuracy assessment of object-based image classification: another STEP. *International Journal of Remote Sensing*, 35(16), 6135–6156. <https://doi.org/10.1080/01431161.2014.943328>
- Lu, D., Weng, Q. (2007). A survey of image classification methods and techniques for improving classification performance. *International Journal of Remote Sensing*, 28(5), 823–870. <https://doi.org/10.1080/01431160600746456>
- Masocha, M., Dube, T., Makore, M., Shekede, M. D., Funani, J. (2018). Surface water bodies mapping in Zimbabwe using landsat 8 OLI multispectral imagery: A comparison of multiple water indices. *Physics and Chemistry of the Earth*, 106(May), 63–67. <https://doi.org/10.1016/j.pce.2018.05.005>
- McFeeters, S. K. (1996). The use of the Normalized Difference Water Index (NDWI) in the delineation of open water features. *International Journal of Remote Sensing*, 17(7), 1425–1432.
- Merry, C. J. (2001). Basic electromagnetic radiation. *Manual of Geospatial Science and Technology*, 62.
- Nazari-Sharabian, M., Ahmad, S., Moses, K. (2018). Climate change and groundwater: a short review. *Climate change and groundwater: a short review. Engineering, Technology and Applied Science Research*, 8(6), 3668–3672. 2
- Otsu, N. (1979). A threshold selection method from gray-level histograms. *IEEE Transactions on Systems, Man, and Cybernetics*, 9(1), 62–66.
- Otukei, J. R., Blaschke, T. (2010). Land cover change assessment using decision trees, support vector machines and maximum likelihood classification algorithms. *International Journal of Applied Earth Observation and Geoinformation*, 12, S27--S31.
- Pandey, B. N., Rana, A., others. (2018). A literature survey of optimization techniques for satellite image segmentation. 2018 *International Conference on*

- Advanced Computation and Telecommunication (ICACAT)*, 1–5.
- Pare, S., Kumar, A., Singh, G. K., Bajaj, V. (2020). Image segmentation using multilevel thresholding: a research review. *Iranian Journal of Science and Technology, Transactions of Electrical Engineering*, 44(1), 1–29.
- Rabinskiy, L. N., Tushavina, O. V., Starovoitov, E. I. (2020). Study of thermal effects of electromagnetic radiation on the environment from space rocket activity. *INCAS Bulletin*, 12, 141–148.
- Sezgin, M., Sankur, B. (2004). Survey over image thresholding techniques and quantitative performance evaluation. *Journal of Electronic Imaging*, 13(1), 146–165.
- Suwarsono, S., Yulianto, F., Fitriana, H. L., Nugroho, U. C., Sukowati, K. A. D., Khomarudin, M. R. (2021). Detecting the surface water area in Cirata dam upstream Citarum using a water index from Sentinel-2. *International Journal of Remote Sensing and Earth Sciences (IJReSES)*, 17(1), 1–8.
- Talukdar, S., Singha, P., Mahato, S., Pal, S., Liou, Y.-A., Rahman, A. (2020). Land-use land-cover classification by machine learning classifiers for satellite observations—A review. *Remote Sensing*, 12(7), 1135.
- Verpoorter, C., Kutser, T., Seekell, D. A., Tranvik, L. J. (2014). A global inventory of lakes based on high-resolution satellite imagery. *Geophysical Research Letters*, 41(18), 6396–6402. <https://doi.org/10.1002/2014GL060641>
- Verpoorter, C., Kutser, T., Tranvik, L. (2012). Automated mapping of water bodies using Landsat multispectral data. *Limnology and Oceanography: Methods*, 10(12), 1037–1050.
- Villamagna, A. M., Murphy, B. R. (2010). Ecological and socio-economic impacts of invasive water hyacinth (*Eichhornia crassipes*): a review. *Freshwater Biology*, 55(2), 282–298.
- Wang, Y., Zang, S., Tian, Y. (2020). Mapping paddy rice with the random forest algorithm using MODIS and SMAP time series. *Chaos, Solitons & Fractals*, 140, 110116.
- Weise, K., Höfer, R., Franke, J., Guelmami, A., Simonson, W., Muro, J., O'Connor, B., Strauch, A., Flink, S., Eberle, J., others. (2020). Wetland extent tools for SDG 6.6. 1 reporting from the Satellite-based Wetland Observation Service (SWOS). *Remote Sensing of Environment*, 247, 111892.
- Xing, L., Niu, Z. (2019). Mapping and analyzing China's wetlands using MODIS time series data. *Wetlands Ecology and Management*, 27(5), 693–710.
- Yan, D., Huang, C., Ma, N., Zhang, Y. (2020). Improved landsat-based water and snow indices for extracting lake and snow cover/glacier in the Tibetan plateau. *Water (Switzerland)*, 12(5). <https://doi.org/10.3390/W12051339>
- Yang, F., Guo, J., Tan, H., Wang, J. (2017). Automated extraction of urban water bodies from ZY-3 multi-spectral imagery. *Water (Switzerland)*, 9(2). <https://doi.org/10.3390/w9020144>
- Yang, P., Song, W., Zhao, X., Zheng, R., Qingge, L. (2020). An improved Otsu threshold segmentation algorithm. *International Journal of Computational Science and Engineering*, 22(1), 146–153.
- Zhai, K., Wu, X., Qin, Y., Du, P. (2015). Comparison of surface water extraction performances of different classic water indices using OLI and TM imageries in different situations. *Geo-Spatial Information Science*, 18(1), 32–42. <https://doi.org/10.1080/10095020.2015.1017911>
- Zhan, X., Sohlberg, R. A., Townshend, J. R. G., DiMiceli, C., Carroll, M. L., Eastman, J. C., Hansen, M. C., DeFries, R. S. (2002). Detection of land cover changes using MODIS 250 m data. *Remote Sensing of Environment*, 83(1–2), 336–350.